Available online at www.sciencedirect.com
ScienceDirect
Journal of Catalysis 248 (2007) 111–119
JOURNAL OF CATALYSIS
www.elsevier.com/locate/jcat

Transformation of a model FCC gasoline olefin over transition monometallic sulfide catalysts

A. Daudin [a], S. Brunet [a,*], G. Perot [a], P. Raybaud [b], C. Bouchy [c]

[a] *UMR CNRS 6503, Catalyse en Chimie Organique, Université de Poitiers, Faculté des Sciences Fondamentales et Appliquées, 40 avenue du Recteur Pineau, 86022 Poitiers Cedex, France*

[b] *IFP, Direction Chimie et Physico-Chimie Appliquées, 1–4 avenue de Bois Préau, 92858 Rueil Malmaison, France*

[c] *IFP, Direction Catalyse et Séparation, BP 3, 69390 Vernaison, France*

Received 15 November 2006; revised 7 March 2007; accepted 11 March 2007

Abstract

The selective HDS of FCC gasoline is a sensible option for reducing sulfur content in commercial gasoline. For such application, a minimum activity of the catalyst toward olefin hydrogenation is required to preserve the high octane number of the feedstock. The conversion of a model FCC olefin (2,3-dimethylbut-2-ene:23DMB2N) under close HDS conditions was investigated over a series of unsupported transition monometallic sulfides (FeS, Ni_3S_2, PdS, Co_9S_8, Rh_2S_3, RuS_2, PtS, and MoS_2). The results reveal for the first time that a volcano curve relationship exists between the ab initio calculated sulfur–metal bond energy, E(MS), descriptor of bulk TMS, and their activities in olefin hydrogenation under the conditions of HDS of FCC gasoline. In particular, Rh_2S_3, with an intermediate metal sulfide bond energy of 119 kJ/mol, was the most active catalyst in hydrogenation of the model olefin. In a similar spirit as volcano curves obtained for the HDS of dibenzothiophene and hydrogenation of toluene and recently reported in the literature, a microkinetic model furnished a rational interpretation of this trend.

Keywords: Hydrogenation; Isomerization; Gasoline; Transition monometallic sulfide catalysts; 2,3-Dimethylbut-2-ene

1. Introduction

Transition monometallic sulfide (TMS) catalysts are known to be active in various hydrotreating reactions [1]. Pecoraro and Chianelli [2] were the first to report a systematic study of the intrinsic activity of bulk TMS in a model reaction, the hydrodesulfurization (HDS) of dibenzothiophene at 400 °C. They established a relative activity scale for TMS as a function of the periodic position of the transition metals. These results were further confirmed by several experimental studies of both unsupported [3] and supported sulfides [3–5] in HDS, hydrodenitrogenation (HDN), and hydrogenation (HYD) of aromatics that found that group VIII metal sulfides of the first row (e.g., Fe, Co, Ni) were poorly active, whereas those of the second row (e.g., Ru, Rh) were much more active. These early results triggered several attempts in the 1980s and 1990s to develop a theoretical foundation for the observed periodic trends in TMS activities, such as TMS enthalpy of formation [2], sulfur coordination number [6], and bond energy model [7].

Recent progress brought by application of density functional theory to realistic models of sulfide catalysts [8] have overcome the limitations of previous approaches in properly investigating the structure and electronic properties of numerous TMS catalysts [9,10]. In particular, a general approach called the "yin-yang" ab initio descriptor rationalized experimental trends observed in HDS and HYD activity of those catalysts [10–12]. This descriptor, termed the bulk sulfur–metal bond energy, E(MS), of the TMS, shows how experimental activity patterns can be correlated with a computed-bond-energy descriptor in accordance with the Sabatier principle [13]. Volcano-type relationships have been established between the ab initio calculated metal–sulfur bond energies, E(MS), and various catalytic activities relevant for hydrotreatment processes, including HDS of dibenzothiophene [10–12,14] and HYD of biphenyl [8,15] and, more recently, toluene [16,17]. Indeed, Pecoraro et al. [2]

* Corresponding author. Fax: +33 549453897.
E-mail address: sylvette.brunet@univ-poitiers.fr (S. Brunet).

0021-9517/$ – see front matter
doi:10.1016/j.jcat.2007.03.009

and Lacroix et al. [3] correlated higher HDS activity of DBT with an optimal E(MS) of 120–140 kJ/mol, and greater HYD activity of biphenyl was obtained for E(MS) of around 110–120 kJ/mol. Consequently, it has become possible to rationalize and predict the performance of sulfide catalysts from such volcano curve relationships. A recent review has described the theoretical advances in this area in more detail [8].

The European Union's planned reduction of the sulfur level in diesel and gasoline to 10 wt ppm in 2009 [18] will required the elaboration of new catalysts or optimization of conventional catalysts. Emissions from motor vehicles (NO_x and SO_x) contribute greatly to air pollution, and sulfur is a well-known poison for catalytic converters. The gasoline fraction produced from the FCC process represents 30–50% of the commercialized motor fuel but contains up to 85–95% of the sulfur impurities. It is composed mainly of aromatics (30 vol%), alkenes (30 vol%), and sulfur compounds such as alkylthiophenes (max. 5000 ppm) [19–21]. These olefins (composed of C_5–C_{10} and mainly C_6 olefins) are iso-olefins and internal double-bond olefins, which are more stable and less reactive than terminal olefins for obtaining and maintaining the octane number. A high hydrotreating selectivity, corresponding to a high HDS activity and a low hydrogenation activity for olefins (HYDO), is required. Indeed, significant alkene saturation can occur during the HDS process, leading to a lower octane number in the final product. Consequently, hydrotreating catalysts must meet selective criteria for HDS/HYDO—that is, achieve deep HDS with minimum olefin saturation.

Recent work [22,23] has shown that the isomerization step may be a key factor in the hydrogenation of alkenes. Indeed, Mey et al. [23] showed that the first step in the transformation of 23DMB2N is its isomerization in 23DMB1N, followed by the hydrogenation step to produce 23DMB.

The selectivity for HDS/HYDO was increased by modifying the acid–base properties of the support either by decreasing the acidity of the support by alkaline elements (e.g., Li, K) [23–25] or using a more basic support such as hydrotalcite [26], or by poisoning selective hydrogenation sites by carbon deposition [27,28] or adsorption of basic nitrogen compounds [29]. Indeed, Mey et al. [23] reported decreased hydrogenation activity on CoMo-supported catalyst modified by potassium. These results have been explained by the inhibition of the olefin isomerization activity and consequent decreased activity of the catalyst in olefin hydrogenation.

To the best of our knowledge, the correlation between the activities of TMS and their corresponding E(MS) descriptor has not yet been investigated for the reaction of alkene hydrogenation. Such a study is of practical and theoretical interest because for MoS_2 catalyst, Qu and Prins [30] suggested that hydrogenation of aromatics occurs on sites different from those active in the hydrogenation of cycloalkenes.

This paper reports the activity of various unsupported TMS (FeS, Ni_3S_2, PdS, Co_9S_8, Rh_2S_3, RuS_2, PtS, and MoS_2) catalysts in the transformation of a model feed composed of 2,3-dimethylbut-2-ene (23DMB2N) in n-heptane in the presence of a partial pressure of H_2S corresponding to 1000 ppm wt of sulfur in the model feed. This alkene is considered representative of olefins found in FCC gasoline. Indeed, an olefin with a branched skeleton and internal double bond that can give rise to a rather limited number of isomers, such as 2,3-dimethyl-2-ene, seems quite appropriate as a model molecule for determining the various mechanisms and active sites involved. A kinetic study using a model molecule should provide more information than a study using a real feed for dissociating the various phenomena involved [19–22]. The TMS catalysts were chosen to cover a representative interval of metal–sulfur bond energies, E(MS), 70–170 kJ/mol, as defined previously [11]. Unsupported TMS catalysts were used to avoid any possible support effect. The reactivity of the olefinic feed was measured under conditions typical of FCC gasoline-selective HDS. Hydrogenation activities with regard to the TMS catalysts evaluated are discussed with the E(MS) descriptor proposed by Toulhoat and Raybaud [11] to explore whether volcano curves may exist for these new classes of reactions, as have been obtained recently for toluene and biphenyl hydrogenation. Furthermore, in the case of 23DMB2N hydrogenation, a microkinetic model to explain the E(MS)-activity relationship is proposed.

2. Experimental

2.1. Catalyst preparation

Co, Ni, Ru, Rh, Pd, and Pt sulfides were prepared using the nonaqueous precipitation method reported by Pecoraro and Chianelli [2]. The metal chloride precursor and lithium sulfide were added in ethyl acetate, and the metal sulfide was obtained after 4 h of stirring at 353 K. Then the solution was cooled to room temperature and filtrated to recover the dark precipitate. The corresponding sulfide solid was stabilized by a sulfidation step in H_2/H_2S (10 mol% H_2S) flow for 2 h at 673 K (heating rate, 276.3 K/min). LiCl was removed by several washes with acetic acid and vacuum filtration. Finally, the metallic sulfide was obtained after a second sulfidation procedure under usual conditions.

Preparation of molybdenum sulfide was carried out by thermal decomposition of ammonium thiomolybdate [31,32]. First, the ammonium tetrathiomolybdate $(NH_4)_2MoS_4$ (ATM) was obtained by reaction between ammonium heptamolybdate $(NH_4)_6[Mo_7O_{24}]\cdot 4H_2O$ (4 g in 20 cc of distilled water) with a 50 wt% of ammonium sulfide $(NH_4)_2S$ in aqueous solution at 333 °C. The ATM precursor was precipitated as red crystals by cooling the solution in iced water for 3 h, after which the precipitated red crystals were thoroughly washed with isopropanol and dried.

2.2. Characterization

The TMS catalysts were characterized before and after catalytic activity measurements by TEM combined with EDX (Philips CM 120 kV), X-ray diffraction (Bruker D5005), BET surface area (Micromeritics ASAP 2010), and elemental analysis (CE Instruments NA2100 Protein) at the University of Poitiers (LACCO) to identify the exact nature of TMS and

Table 1
XPS binding energies of the various TMS

TMS	Binding energy (eV)	
	Metal	Sulfur ($2p_{3/2}$)
MoS_2	$3d_{5/2}$: 229.4	162.2
(MoO_x)	$3d_{5/2}$: 232.5	–
FeS	$2p_{3/2}$: 706.6	162
Ni_3S_2	$2p_{3/2}$: 852.4	162.1
Co_9S_8	$2p_{3/2}$: 778.3	162.3
PdS	$3d_{5/2}$: 336.3	161.6
RuS_2	$3d_{5/2}$: 280	162.0

verify that no modification was done after the activity measurements. Comparison of the XRD patterns and the JCPDS database allowed identification of the various crystalline TMS phases.

XPS spectra were recorded using a KRATOS AXIS Ultra spectrometer equipped with a 300 W Al$K\alpha$ source ($h\nu =$ 1486.6 eV). TMS samples were packed in Shlenk under argon to avoid sulfate formation. They were identified with reference samples drawn from the Handbook of X-Ray Photoelectron Spectroscopy [33], NIST X-ray Photoelectron Spectroscopy Database (NIST Standard Reference Database 20, Web Version 3.4).

Calibration was done with the carbon peak of contamination identified at 284 eV. For each TMS, the metal and sulfur peaks were identified with their binding energies (Table 1). The elemental surface composition of the TMS and thus the atomic ratio of sulfur/metal (S/Me) after reaction were determined (with a relative uncertainty of 20%) from the intensity of the metal and sulfur peaks.

2.3. Reaction conditions

Catalytic activity measurements were carried out in a fixed-bed reactor at 523 K under a total pressure of 2 MPa. The catalyst was presulfided at 673 K for 10 h with a mixture of 10 mol% H_2S in H_2 under atmospheric pressure and then cooled to the reaction temperature in the presence of the sulfiding mixture. The desired reaction conditions were adjusted, and the model feed was injected into the reactor. The model feed was composed of 20 wt% 23DMB2N in n-heptane. The residence time varied from 0.24 (3.3 g 23DMB2N/g cata/s) to 164 s (4.9×10^{-3} g 23DMB2N/g cata/s). The H_2/feed ratio was 360 L/L.

All experiments were performed in the presence of H_2S to maintain the various catalysts in a sulfided state. The partial pressure of H_2S (1.9 kPa) chosen corresponded to a equivalent of 1000 wt ppm S in the feed, a typical value for European FCC gasoline. All partial pressures conditions of the various components for sulfidation step and catalytic activity measurements are reported in Table 2.

For accurate activity measurements, residence times were chosen so as to also keep the overall conversion of 23DMB2N into 23DMB1N (isomerization [Isom]) and into 23DMB (HYDO) nearly constant around 15% in both cases. Nevertheless, for the more active TMS, two different experiments were necessary under conditions in which linear relationships between conversions and contact time were obtained. Activity of the TMS in isomerization is defined as the number of moles of 23DMB1N formed per second per square meter of catalyst, and activity of the TMS in HYDO is defined as the number of moles of 23DMB formed per second per square meter of catalyst.

Table 2
Partial pressures of the different components for the preliminary sulfidation step and the transformation of 23DMB2N

Pressure (bar)	Sulfidation	Feed
P_{olefin}	0	1.51
P_{H_2S}	0.1	0.02
P_{H_2}	0.9	13.40
P_{nC_7}	0	5.07
P_{total}	1	20

Table 3
Products resulting from the transformation of 23DMB2N

Isomerization (Isom)

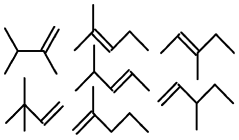

Hydrogenation (HYDO)

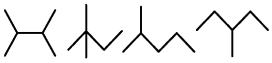

2.4. Analysis

The reaction products were analyzed online using a Varian 3800 gas chromatograph equipped with an automatic sampling valve, a 50-m PONA (HP) capillary column (i.d., 0.2 mm; film thickness, 0.5 μm), a flame ionization detector, and a cryogenic system. Analytical conditions were taken from previous work [23] to obtain accurate separation: a temperature program from 273 K (15 min) to 293 K (274.3 K/min), from 293 to 323 K (275 K/min), and then from 323 to 423 K (280 K/min). Product identification was performed by GC-MS coupling (Finnigan INCOS 500). The products of transformation of 2,3-dimethylbut-2-ene are reported in Table 3. Products obtained in our experimental conditions for the various TMS were in agreement with previous findings with commercial $CoMo/Al_2O_3$ catalyst.

Transformation of the 2,3-dimethylbut-2-ene (23DMB2N) led to the formation of isomerization products (mainly 2,3-dimethylbut-1-ene [23DMB1N]) and hydrogenation products (mainly 2,3-dimethylbutane [23DMB]). Thiols were not observed under our experimental conditions. It should be emphasized that the limit of detection for such compounds was estimated as ca. 10 ppm wt with the GC analysis. Consequently, it was possible to successively measure isomerization activity (with 23DMB1N formation <30% corresponding to the thermodynamic equilibrium between 23DMB2N and 23DMB1N under the experimental conditions [22,34]) and hydrogenation activity (with the formation of 23DMB).

2.5. Microkinetic modeling

For aromatic (e.g., biphenyl, toluene) HYD and dibenzothiophene HDS over sulfide catalysts, an approach combining sulfur–metal bond energy ab initio descriptor and microkinetic modeling has proven successful [8,11,16,17]. These results suggest a general interpretation of periodic trends in catalysis by sulfides. To explore whether such a concept holds for olefin hydrogenation, we tested several possible models and identified the one best able to reproduce the experimental catalytic results. In previous works [11,16,17] ab initio microkinetic models within the Langmuir–Hinshelwood formalism put forward that $E(\mathrm{MS})$, as defined previously [10–12], appears to be a relevant chemical descriptor of the catalyst for recovering volcano curve relationships for catalytic activity. To keep the formalism as general as possible, the model proposed in the current work is a one-site model and assumes that H_2S and H_2 adsorb dissociatively at the surface, as suggested earlier [35]. The sulfhydryl groups created by H_2S dissociation take part in the elementary steps of the reaction. In what follows, we describe the proposed microkinetic model for olefin hydrogenation reaction. This model is optimized by assuming a linear relationship between adsorption constants or activation energies and the sulfur–metal bond energies calculated by DFT in previous work [10–12]; the approach is directly inspired by Brønsted–Evans–Polanyi (BEP) formalism.

2.5.1. Elementary steps of the mechanism

Equations (E0)–(E6) are the relevant elementary steps of the mechanism involved in the one-site (M^*) microkinetic model of olefin hydrogenation:

$$M^* + H_2S \overset{K_S}{\longleftrightarrow} MS + H_2, \tag{E0}$$

$$MS + M^* + H_2 \overset{K_{H_2}}{\longleftrightarrow} MSH + MH, \tag{E1}$$

$$MS + M^* + H_2S \overset{K_{H_2S}}{\longleftrightarrow} 2MSH, \tag{E2}$$

$$M^* + R \overset{K_R}{\longleftrightarrow} MR, \tag{E3}$$

$$MR + MSH \overset{K_{SH}}{\longrightarrow} MRH + MS, \tag{E4}$$

$$MRH + MH \rightarrow MRH_2 + M^*, \tag{E5}$$

$$MRH_2 \rightarrow RH_2 + M^*. \tag{E6}$$

Note that step (E0), corresponding to the creation of MS species from the M^* site, is directly related to the sulfidation equilibrium state of the catalytic surface, depending on the sulforeductive conditions as revealed by DFT calculations [36,37]. Indeed, the possibility that the effect of HDS reaction conditions change this surface state characterized by the distribution of MS and M^* species cannot be excluded. At the same time, this equation assuming a link between MS and M^* avoids the need to consider a more complex model with two independent sites. We also tested such a two-site model but found that it did not improve the final fit.

Hydrogen and H_2S are both activated through heterolytic dissociation at steps (E1) and (E2). Step (E3) represents adsorption of the 23DMB2N olefin, labelled as R. Step (E4) is the initial hydrogen transfer from the sulfhydryl group to the adsorbed olefin and is assumed to be rate-determining (for the optimal model). Step (E5) is the second hydrogenation from a MH species. Finally, step (E6) corresponds to alkane desorption with simultaneous regeneration of M^* sites. To equilibrate the global reaction scheme (with full M^* recovery and avoiding H_2S overconsumption), the following terminating step is proposed:

$$2MSH + H_2 \rightarrow 2M^* + 2H_2S. \tag{E7}$$

Consequently, H_2S takes part in the reaction by producing the MS and MSH species at the surface and is regenerated at the end of the catalytic cycle, so it does not appear in the global reaction. This model is the one leading to the best fit of the experimental results. Among other models tested but not reported here (for the sake of clarity) and explored previously [38], we have verified that assuming a different rate-determining step [such as (E5)] and/or inverting the hydrogenation steps (E4) and (E5) leads to less satisfactory results.

2.5.2. Equation rates and Brønsted–Evans–Polanyi relationships

Within the proposed mechanism, steps (E0)–(E4) are assumed to be equilibrated, whereas step (E5), corresponding to the addition of the first hydrogen from the sulfhydryl group, is rate-determining. The equation of site conservation is written as

$$\theta^* + \theta_S + \theta_{SH} + \theta_H + \theta_R = 1. \tag{1}$$

The reaction rate is expressed as

$$r(T, p_{H_2S}, p_{H_2}) = k_{SH}\theta_R\theta_{SH} = k_{SH}\frac{\alpha_R\alpha_S^{1/2}\alpha_{H_2S}^{1/2}}{(1+\alpha_S+\alpha_R+\alpha_S^{1/2}\alpha_{H_2S}^{1/2}+\alpha_{H_2}\alpha_S^{1/2}\alpha_{H_2S}^{-1/2})^2} \tag{2}$$

with

$$\alpha_i = K_i\frac{p_i}{p^0} \quad \text{and} \quad \alpha_S = \frac{p_{H_2S}}{K_S p_{H_2}}. \tag{3}$$

To improve the model fit, an additional term of thermal conversion, rth, is included for plotting rate equation (2). This contribution, which is negligible for most of the active systems and does not depend on $E(\mathrm{MS})$, accounts for the very low (but different from zero) TOF of catalysts with very low/high $E(\mathrm{MS})$.

In the same spirit as proposed earlier [10,17], the adsorption constants, K_i, and activation energies are expressed as a function of a relevant intrinsic parameter of the sulfide catalyst, the $E(\mathrm{MS})$, as defined in [10–12]. The adsorption constants, K_i, and the kinetic constant k_{SH} are thus written as

$$K_i = e^{\Delta S_i/R - \Delta H_i/RT} = e^{\Delta S_i/R} e^{[\Delta E_{i,0} + \beta_i E(\mathrm{MS})]/RT} \tag{4}$$

and

$$k_{SH} = \frac{k_B T}{h} e^{-\Delta G^{\neq}/RT} = \frac{k_B T}{h} e^{-[\Delta G_0^{\neq} + \gamma_{SH} E_{(\mathrm{MS})}]/RT}, \tag{5}$$

where k_B and h are the Boltzmann and Planck constants, respectively.

If a linear relationship holds between the adsorption energy variation (respectively activation energy) and $E(\mathrm{MS})$, resulting

from Brønsted–Evans–Polanyi (BEP) relationships [39–41], then K_i and k_{SH} depend on the catalyst via $E(MS)$ and the BEP parameters, β_i and γ_{SH}, depending on the adsorbed molecules i. Equation (2) is finally a parameterized expression of r depending on T, p_{H_2}, p_{H_2S}, and $E(MS)$. Achieving optimal fit of the BEP parameters involves minimizing the deviation of the theoretical values given by Eq. (2) from the experimental HYD activities.

Finally, from the rate law's expression, it is possible to extract an estimated value of apparent activation energies, E_{app}, as

$$r\left(T, p_{H_2S}, p_{H_2}, E(MS)\right) = Ae^{-E_{app}/RT}, \quad (6)$$

where A is the apparent prefactor. For given (T, p) reaction conditions, the model allows determination of the variation of E_{app} as a function of $E(MS)$.

3. Results and discussion

3.1. Characterization of the TMS catalysts

The crystalline structure, stoichiometry, and surface areas of the different monometallic TMS catalysts are given in Table 4. Their respective compositions, according to chemical analysis and XRD pattern, correspond to FeS, PdS, Co_9S_8, Rh_2S_3, RuS_2, PtS, and MoS_2 [2,31,32]. A mixture of two phases, Ni_9S_8 and NiS, was observed for the nickel sulfide. FeS, PdS, Co_9S_8, Rh_2S_3, RuS_2, and PtS have similar specific surface areas (around 30 m^2/g); nickel sulfide and palladium sulfide have the lowest specific surface areas (5 m^2/g), and MoS_2 has the highest (80 m^2/g).

Traces of chlorine (<1 wt%) were detected in all of the catalysts prepared by the nonaqueous method.

After catalytic activity evaluation by X-ray diffraction, elemental analysis, and XPS, all of the catalysts were characterized to show the stability of the TMS (Table 5). No modification of structure during the activity measurement was noted except for the reduction of nickel sulfides (Ni_9S_8, NiS) in Ni_3S_2 sulfide phase. This was also in accordance with the decrease of the sulfur/metal ratio from 0.9 before the test to 0.5 after the test as measured by XPS. For the other unsupported TMS, XPS results also confirmed a similar composition of the catalyst surface and the bulk. The carbon content was relatively low, 0.4–1 wt%, for all TMS except MoS_2, which had a higher content (about 5 wt%), in accordance with its significantly higher surface area. These results demonstrate the occurrence of carbon deposition during the experiment.

Table 4
Physico-chemical properties of the unsupported monometallic TMS determined by XRD, elemental analysis and specific surface area

Metal (Me)	TMS	S/Me atom	Specific surface area (m^2/g)
Fe	FeS	0.7	20
Ni	Ni_9S_8, NiS	0.9	3
Co	Co_9S_8	0.9	22
Pd	PdS	0.8	5
Rh	Rh_2S_3	1.7	26
Ru	RuS_2	1.9	29
Pt	PtS	1.1	29
Mo	MoS_2	2.2	80

3.2. Transformation of 23DMB2N over sulfides catalysts

Fig. 1 shows the formation of the main products versus residence time over rhodium sulfide: 2,3-dimethylbut-1-ene (23DMB1N: main isomerization product) and the formation of 2,3-dimethylbutane (23DMB: main hydrogenation product). Skeletal isomerization products and their hydrogenation products were also detected in very small amounts (about 1 mol%). Similar results were obtained for all of the TMS catalysts evaluated.

As reported previously [42], the isomerization of 23DMB2N into 2,3-dimethylbut-1-ene (23DMB1N) over supported CoMo catalyst occurred readily under the conditions of the reaction, and thermodynamic equilibrium between the two isomers was reached rapidly (residence times <0.2 s). Consequently, the equilibrium mixture of both isomers (23DMB2N + 23DMB1N) is considered the reactant when measuring the hydrogenation activity of the catalysts. After 0.2 s of residence time, 23DMB became the main product. 23DMB2N also led to various minor products (skeletal products). The reac-

Table 5
Comparison of the characterization of the various TMS before (by XRD and elemental analysis) and after the transformation of 23DMB2N (by XRD and XPS)

TMS before catalytic activity measurement		TMS after catalytic activity measurement		
TMS	S/Me atom	TMS	C (wt%)	S/Me atom
FeS	0.7	FeS	1.3	1.1
Ni_9S_8, NiS	0.9	Ni_3S_2	0.4	0.5
Co_9S_8	0.9	Co_9S_8	0.7	0.9
PdS	0.8	PdS	0.4	1
Rh_2S_3	1.7	Rh_2S_3	0.8	–
RuS_2	1.9	RuS_2	1.1	1.9
PtS	1.1	PtS	1.1	1
MoS_2	2.2	MoS_2	2.6	1.8

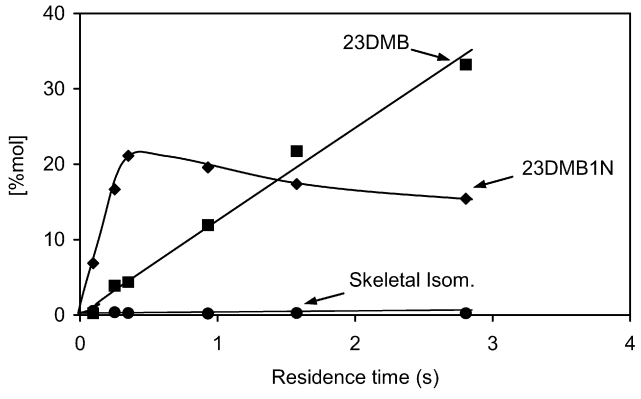

Fig. 1. Transformation of 23DMB2N over rhodium sulfide (Rh_2S_3). Formation of 2,3-dimethylbut-1-ene (23DMB1N), 2,3 dimethylbutane (23DMB) and products resulting of skeletal isomerization ($T = 523$ K, $P = 2$ MPa, H_2/feed = 360 L/L).

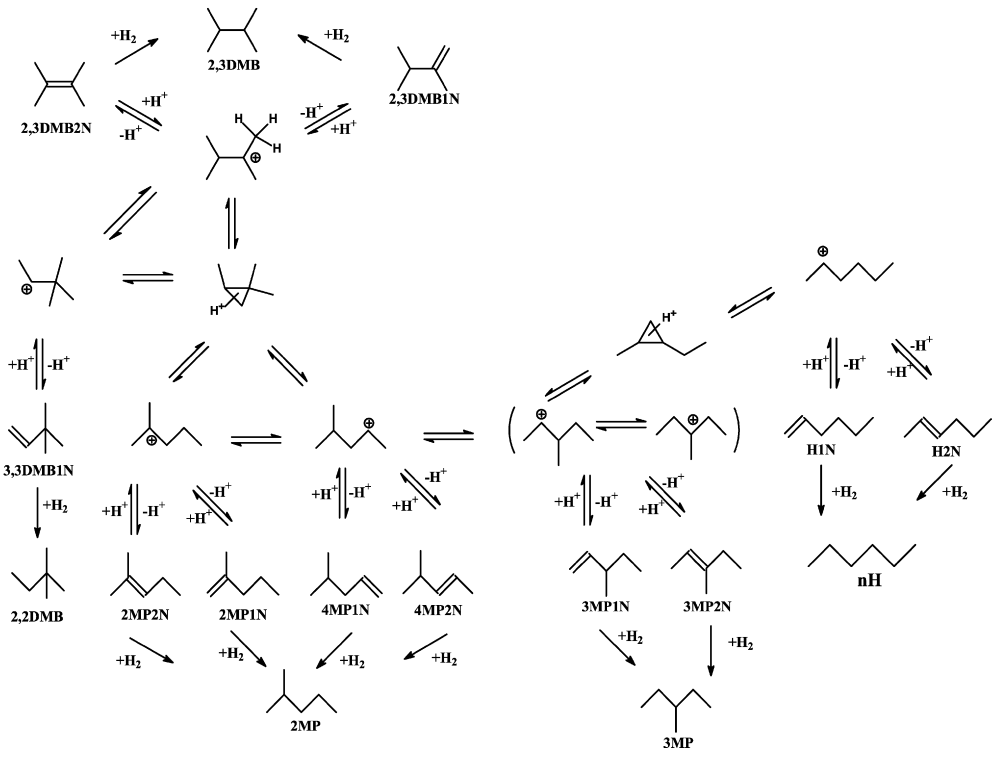

Scheme 1. 23DMB2N transformation, isomerization and hydrogenation products. 23DMB2N, 2,3-dimethylbut-2-ene; 23DMB1N, 2,3-dimethylbut-1-ene; 33DMB1N, 3,3-dimethylbut-1-ene; 2MP1N, 2-methylpent-1-ene; 2MP2N, 2-methylpent-2-ene; 4MP1N, 4-methylpent-1-ene; 4MP2N, 4-methylpent-2-ene; 3MP1N, 3-methylpent-1-ene; 3MP2N, 3-methylpent-2-ene; 22DMB, 2,2-dimethylbutane; 2MP, 2-methylpentane; 3MP, 3-methylpentane [23].

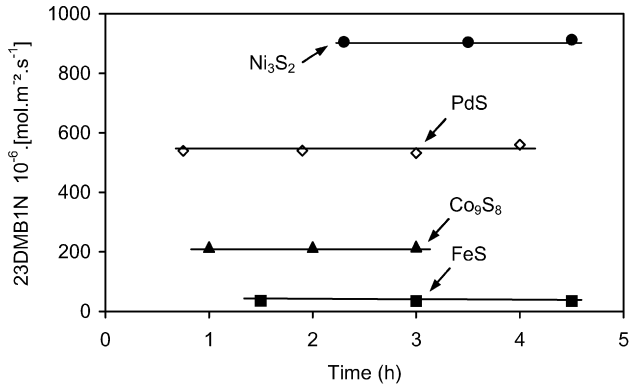

Fig. 2. Transformation of 23DMB2N over Ni_3S_2, PdS, Co_9S_8, FeS. Activity of the formation of 23DMB1N ($T = 523$ K, $P = 2$ MPa, H_2/feed = 360 L/L).

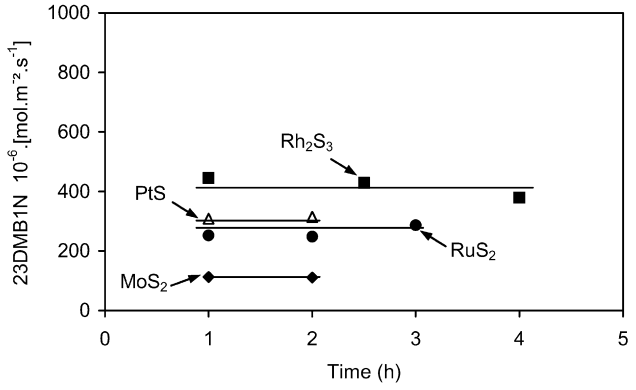

Fig. 3. Transformation of 23DMB2N over Rh_2S_3, PtS, RuS_2, MoS_2. Activity of the formation of 23DMB1N ($T = 623$ K, $P = 2$ MPa, H_2/feed = 360 L/L).

tional scheme of 23DMB2N transformation established over a commercial CoMo supported catalyst in a previous work [22] (Scheme 1) was in agreement with the product distribution observed over unsupported TMS.

For all sulfides studied, we report the evolution of the activities for the isomerization (formation of 23DMB1N, Figs. 2 and 3) and hydrogenation reactions (formation of 23DMB, Figs. 4 and 5) versus time on stream. No deactivation was noted during the isomerization step for any of the TMS catalysts. For the hydrogenation step, all of the TMS catalysts but nickel sulfide exhibited a more or less longer deactivation time, followed by stabilization after 5–20 h. Indeed, PdS had the longest deactivation and stabilization period, more than 24 h. All of the other TMS catalysts stabilized after roughly 10 h. In each case, the hydrogenation activity was determined from 23DMB formation when stabilization was reached. For the isomerization step (measured by the formation of 23DMB1N), the most active sulfide phase was Ni_3S_2, followed by PdS, Rh_2S_3, PtS, RuS_2, Co_9S_8, and MoS_2. Conversely, for the hydrogenation step (measured by the formation of 23DMB), Rh_2S_3 was the most active phase, followed by RuS_2, PtS, MoS_2, PdS, Co_9S_8, Ni_3S_2, and FeS.

3.3. Relationship between hydrogenation catalytic activity with the metal–sulfur bond energy descriptor

The evolution of the hydrogenation activity as a function of the E(MS) descriptor is shown in Fig. 6. The activity fol-

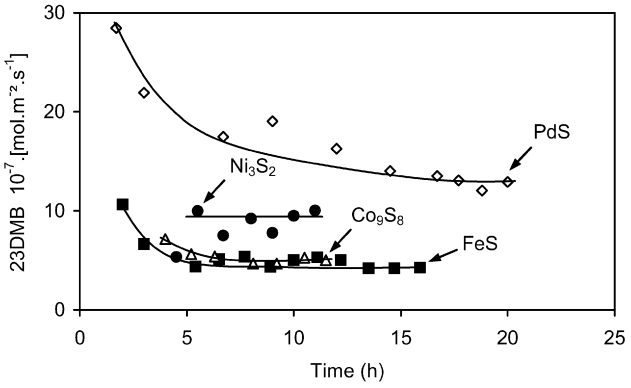

Fig. 4. Transformation of 23DMB2N over Ni_3S_2, PdS, Co_9S_8, FeS. Activity of the formation of 23DMB ($T = 523$ K, $P = 2$ MPa, H_2/feed = 360 L/L).

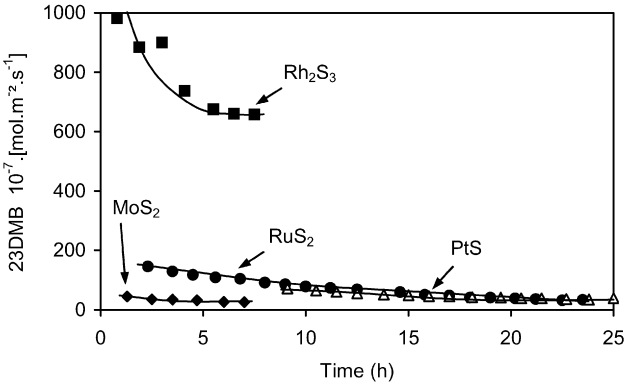

Fig. 5. Transformation of 23DMB2N over Rh_2S_3, PtS, RuS_2, MoS_2. Activity of the formation of 23DMB ($T = 623$ K, $P = 2$ MPa, H_2/feed = 360 L/L).

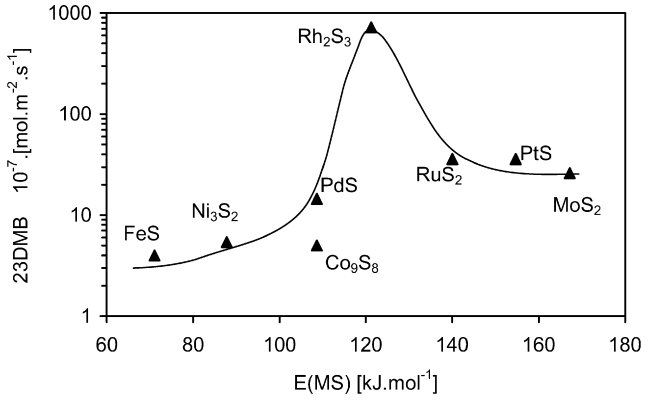

Fig. 6. Transformation of 23DMB2N over various unsupported monometallic sulfides. Hydrogenation activity (mol m^{-2} s^{-1}) (measured by the formation of 23DMB) versus the monometallic bulk sulfur–metal bond energy E(MS) ($T = 523$ K, $P = 2$ MPa, H_2/feed = 360 L/L).

Table 6
Transformation of 23DMB2N—hydrogenation and isomerisation activities of the various TMS

TMS	Activity isom $10^{-7} \times$ (mol m^{-2} s^{-1})	Activity HYDO $10^{-7} \times$ (mol m^{-2} s^{-1})	Isom/HYDO
FeS	170	4	43
Ni_3S_2	9000	5	1800
Co_9S_8	2160	5	432
PdS	5430	14	388
Rh_2S_3	3790	720	5
RuS_2	2500	36	69
PtS	3120	36	87
MoS_2	1120	26	43

lows a volcano-type curve from iron sulfide [lowest E(MS)] to molybdenum sulfide [highest E(MS)]. Indeed, rhodium sulfide (119 kJ/mol) has the highest hydrogenation activity. More particularly, Rh_2S_3 exhibits the highest hydrogenation activity, between 25 times (RuS_2, PtS, MoS_2) and 180 times (FeS, Ni_3S_2, Co_9S_8) higher than the other TMS catalysts. These new results suggest that the volcano curve concept previously reported in the literature for the hydrogenation of aromatics [3,8,16,17] can be extended to olefin hydrogenation. In both cases, a volcano curve relationship was put forward between hydrogenation activity of the different TMS catalysts and the ab initio E(MS) descriptor, with an optimum at 119 kJ/mol corresponding to Rh_2S_3. Whatever the unsaturated compounds (23DMB2N or biphenyl and toluene), the hydrogenation activity follows a similar trend as a function of the E(MS) descriptor. Sulfides with E(MS) < 119 kJ/mol (e.g., FeS, Co_9S_8, Ni_3S_2) exhibit the lowest hydrogenation activity. Rhodium sulfide [with E(MS) = 119 kJ/mol] has the highest activity. Finally, sulfides with higher E(MS) also exhibit weak hydrogenation activity. A microkinetic modelling-based interpretation of this trend is proposed in Section 3.4.

It should also be emphasized that for all of the unsupported TMS catalysts evaluated except Rh_2S_3, the isomerization activity is at least 10 times higher than the hydrogenation activity (Table 6). This finding likely implies that for supported catalysts, neutralization of the acidic sites of the support alone is not sufficient to avoid the isomerization from internal olefins to external olefins, because external olefins are more reactive toward hydrogenation.

3.4. Microkinetic modeling

The BEP linear relationships between adsorption energies [steps (E0)–(E3)] or activation energies of step (E4) and E(MS) used for the kinetic modeling are plotted in Fig. 7. As expected, all adsorption energies are exothermic. The higher the E(MS), the stronger the interaction of the active free site M* with 23DMB2N, –S, –SH. The trend in adsorption energies is rather close to that obtained for toluene hydrogenation [17].

Assuming such BEP relationships, a volcano curve is recovered for the olefin hydrogenation on the tested sulfide catalysts, as shown in Fig. 8. The model is also able to reproduce the non-symmetrical volcano shape, revealing a less pronounced rate decrease on the right side of the volcano compared with the left side. As indicated previously, this trend and the overall fit cannot be correctly rendered by any other model tested in the present study, for instance, assuming step (E5) as the rate-determining step and/or inverting steps (E4) and (E5). We confirm that Rh_2S_3 is the optimum catalyst for intermediate values of E(MS). This result can be interpreted within the framework of the Sabatier principle and the analysis of the surface distribution of the different species as a function of E(MS).

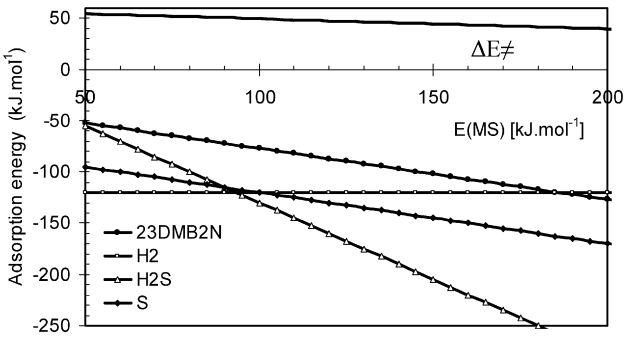

Fig. 7. Linear BEP relationships between adsorption energies (steps (E0)–(E4)) and the activation energy (step (E4)) and the sulfur–metal bond energies, E(MS).

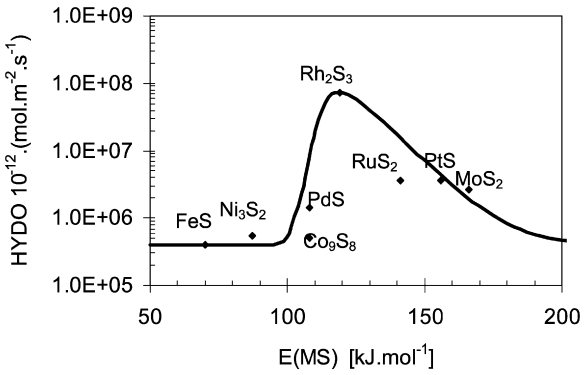

Fig. 8. Microkinetic model according to Eq. (2) best fitting the experimental olefin hydrogenation activities plotted against sulfur–metal bond energies, E(MS), in HDS conditions.

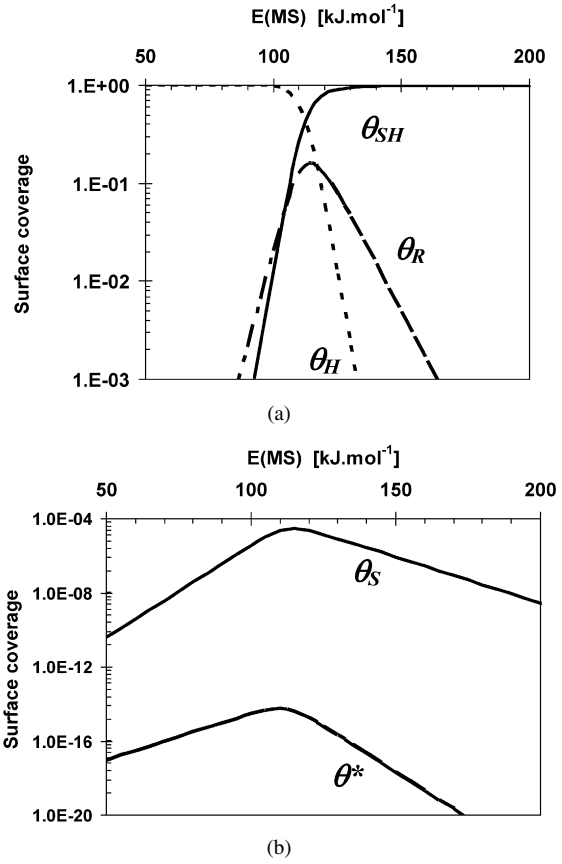

Fig. 9. Surface coverages of the different species as a function of E(MS): (a) most predominant species: 23DMB2N (θ_R), MSH (θ_{SH}) and MH (θ_H); (b) less predominant species: M* (θ^*) and MS (θ_S).

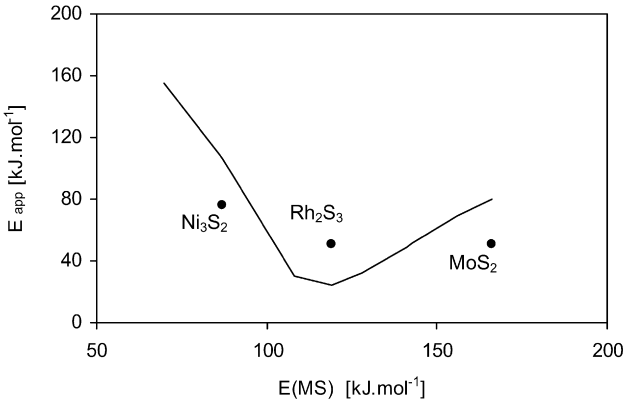

Fig. 10. Apparent activation energies as a function of E(MS). Line: value given by the model, dots: experiments.

Fig. 9a shows that for high E(MS), the surface is saturated by MSH species, and for low E(MS), the surface is fully covered by MH species. These two extreme regions correspond to very low numbers of 23DMB2N molecules adsorbed on the surface. As expected from Eq. (2), the rate decreases when θ_R is low at both high and low E(MS). The fact that the rate-determining step involves hydrogenation of the adsorbed olefin by MSH species saturating the surface at high E(MS) implies that the rate decrease is less pronounced on the right side of the volcano. The 23DMB2N coverage reaches a maximum for intermediate E(MS). At the same time, sulfhydryl species coverage remains high at the surface, which maximizes the product $\theta_{SH}\theta_R$ and explains why the maximum HYD rate is obtained for intermediate E(MS) values such as found for Rh_2S_3. Also note that in this intermediate region, MH species also occupy a nonnegligible fraction of catalytic sites. The nonpredominant MS and M* species also exhibit a maximum for intermediate E(MS) values (Fig. 9b). Hence, the intermediate sulfur–metal bond strength region provides the widest diversity of adsorbed chemical species, which is an optimal situation for heterogeneous catalysis, as has been suggested by Kasztelan [43].

Finally, we have estimated from the rate law given by Eq. (2) the apparent activation energy, E_{app}, resulting from the kinetic modeling. Fig. 10 depicts the variation of E_{app} as a function of E(MS). The values of E_{app} were determined experimentally for three relevant TMS catalysts: Ni_3S_2, Rh_2S_3, and MoS_2. According to the model, the variation of E_{app} exhibits a minimum close to Rh_2S_3, with a more pronounced increase of E_{app} at low E(MS) than at high E(MS). This trend is consistent with the volcano curve discussed earlier. The experimental values reveal an increased E_{app} at low E(MS) but an apparently constant E_{app} at high E(MS). Because the accuracy of experimental activation energies depends on well-controlled (T, p) conditions for determining these energies, perhaps we should not expect better agreement between theoretical and experimental values of apparent kinetic parameters.

4. Conclusion

Based on our findings, we can conclude that it is possible to generalize the volcano curve relationship between the ab initio calculated metal–sulfur bond energy [E(MS)] of various unsupported TMS catalysts and their activity to the hydrogenation of olefins, such as 23DMB2N, under conditions typical of the selective HDS of FCC gasoline. To the best of our knowledge, this is the first time that such a volcano curve has been obtained for this type of important reaction. In particular, Rh_2S_3, with an intermediate metal–sulfide bond energy of 119 kJ/mol, was the most active catalyst for the hydrogenation. The microkinetic modeling combining ab initio metal–sulfur bond energy, E(MS), and BEP formalism allowed a rational interpretation of the volcano curve pattern obtained for olefin HYD. Analysis of adsorbed species coverages show that the maximum of the volcano correspond to the region where the widest chemical diversity of the surface is provided.

Such a rational trend offers new ways of exploring the selectivity of sulfides catalysts. We are currently further investigating the activity of these TMS catalysts for the transformation of a model feed of FCC gasoline to assess whether the selectivity of TMS also can be rationalized using microkinetic modeling combining E(MS) and BEP formalism.

Acknowledgments

A. Daudin thanks the IFP and CNRS for a doctoral grant. The authors also thank P. Lecour and C. Legens for the XPS analysis (IFP Lyon) and fruitful discussions.

References

[1] H. Topsøe, B.S. Clausen, F.E. Massoth, in: J.R. Anderson, M. Boudard (Eds.), Hydrotreating Catalysis, Science and Technology, Springer-Verlag, Berlin, 1996, p. 1.
[2] T.A. Pecoraro, R.R. Chianelli, J. Catal. 67 (1981) 430.
[3] M. Lacroix, H. Marrakchi, C. Calais, M. Breysse, C. Forquy, Stud. Surf. Sci. Catal. 59 (1991) 277.
[4] J.P.R. Vissers, C.K. Groot, E.M. van Oers, V.H.J. de Beer, R. Prins, Bull. Soc. Chim. Belg. 93 (1984) 813.
[5] M.J. Ledoux, O. Michaux, J. Agostini, P. Panissod, J. Catal. 102 (1986) 275.
[6] E.J.M. Hensen, H.J.A. Brans, G.M.H.J. Lardinois, V.H.J. de Beer, J.A.R. van Veen, R.A. van Santen, J. Catal. 192 (2000) 98.
[7] J.K. Nørskov, B.S. Clausen, H. Topsøe, Catal. Lett. 13 (1992) 1.
[8] P. Raybaud, Appl. Catal. A Gen. 322 (2007) 76–91.
[9] R.R. Chianelli, G. Berhault, P. Raybaud, S. Kasztelan, J. Hafner, H. Toulhoat, Appl. Catal. A Gen. 227 (2002) 83.
[10] P. Raybaud, J. Hafner, G. Kresse, H. Toulhoat, J. Phys. Condens. Matter 9 (1997) 11107.
[11] H. Toulhoat, P. Raybaud, J. Catal. 216 (2003) 63.
[12] H. Toulhoat, P. Raybaud, S. Kasztelan, G. Kresse, J. Hafner, Catal. Today 50 (1999) 629.
[13] P. Sabatier, Ber. Dtsch. Chem. Ges. 44 (1911) 2001.
[14] R.R. Chianelli, T.A. Pecoraro, T.R. Halbert, W.H. Pan, E.I. Stiefel, J. Catal. 86 (1984) 226.
[15] M. Lacroix, N. Boutarfa, C. Guillard, M. Vrinat, M. Breysse, J. Catal. 120 (1989) 473.
[16] N. Guernalec, T. Cseri, P. Raybaud, C. Geantet, M. Vrinat, Catal. Today 98 (2004) 61.
[17] N. Guernalec, C. Geantet, P. Raybaud, M. Aouine, T. Cseri, M. Vrinat, Oil Gas Sci. Technol. Rev. IFP 61 (2006) 515.
[18] Off. J. Eur. Commun. L76 (2003) 10.
[19] S. Hatanaka, M. Yamada, O. Sadakane, Ind. Eng. Chem. Res. 36 (1997) 1519.
[20] S. Hatanaka, M. Yamada, O. Sadakane, Ind. Eng. Chem. Res. 36 (1997) 5110.
[21] S. Hatanaka, M. Yamada, O. Sadakane, Ind. Eng. Chem. Res. 37 (1998) 1748.
[22] S. Brunet, D. Mey, G. Pérot, C. Bouchy, F. Diehl, Appl. Catal. A Gen. 278 (2005) 143.
[23] D. Mey, S. Brunet, C. Canaff, F. Maugé, C. Bouchy, F. Diehl, J. Catal. 227 (2004) 436.
[24] J.T. Miller, W.J. Reagan, J.A. Kaduck, J. Kropf, J. Catal. 193 (2000) 123.
[25] C. Sudhakar, M.R. Cesar, R.A. Heinrich, U.S. patent 5 525 211 (1996) to Texaco.
[26] P.S.E. Dai, D.E. Sherwood Jr., R.H. Petty, U.S. patent 5 340 466 (1994) to Texaco.
[27] O. Sadakane, EP 0 745 660 A1 (1996) to Mitsubishi Oil Corporation.
[28] S. Hatanaka, Catal. Surv. Asia 9 (2005) 87.
[29] S. Hatanaka, O. Sadakane, U.S. patent 6 120 679 (2000) to Mitsubishi Oil Corporation.
[30] L. Qu, R. Prins, Appl. Catal. A Gen. 250 (2003) 105.
[31] G. Berhault, A. Mehta, A.C. Pavel, J. Yang, L. Redon, M.J. Yacaman, L.C. Araiza, A.D. Moller, R.R. Chianelli, J. Catal. 198 (2001) 9.
[32] Y. Iwata, K. Sato, T. Yoneda, Y. Miki, Y. Sugimoto, A. Nishijma, H. Shimada, Catal. Today 45 (1998) 353.
[33] C.D. Wagner, W.M. Riggs, L.E. Davis, J.F. Moulder, in: G.E. Muilenberg (Ed.), Handbook of X-Ray Photoelectron Spectroscopy, Perkin–Elmer, Norwalk, CT, 1979.
[34] M. Guisnet, P. Canesson, R. Maurel, Bull. Soc. Chim. Fr. 10 (1970) 3566.
[35] S. Kasztelan, Hydrotreating Technology for Pollution Control, Dekker, New York, 1996, p. 29.
[36] P. Raybaud, J. Hafner, G. Kresse, S. Kasztelan, H. Toulhoat, J. Catal. 189 (2000) 129.
[37] P. Raybaud, J. Hafner, G. Kresse, S. Kasztelan, H. Toulhoat, J. Catal. 190 (2000) 128.
[38] (a) S. Kasztelan, D. Guillaume, Ind. Eng. Chem. Res. 33 (1994) 203; (b) S. Kasztelan, D. Guillaume, Ind. Eng. Chem. Res. 34 (1995) 1500.
[39] J.N. Brønsted, K.J. Pedersen, Z. Phys. Chem. 108 (1924) 185.
[40] M.G. Evans, M. Polanyi, Trans. Faraday Soc. 32 (1936) 1333.
[41] M.G. Evans, M. Polanyi, Trans. Faraday Soc. 11 (1938) 34.
[42] D. Mey, S. Brunet, G. Pérot, F. Diehl, S. Kasztelan, Am. Chem. Soc. Prepr. Div. Pet. Chem. 47 (1) (2002) 69.
[43] S. Kasztelan, Catal. Lett. 2 (1989) 165.